Pure Appl. Chem., Vol. 77, No. 6, pp. 925–945, 2005.
DOI: 10.1351/pac200577060925

Carotenoid–chlorophyll complexes: Ready-to-harvest*

Harsha M. Vaswani†, Nancy E. Holt†, and Graham R. Fleming‡

Department of Chemistry, University of California, and Physical Biosciences Division, Lawrence Berkeley National Laboratory, Berkeley, CA 94720, USA

Abstract: The fundamental interactions between naturally occurring pigments in light-harvesting systems are responsible for the high efficiency of the photosynthetic apparatus. We describe the role of carotenoids (Cars) in light-harvesting systems, including our work elucidating the mechanism of energy transfer from the optically dark Car singlet excited state (S_1) to chlorophyll (Chl) and calculations on the electronic structure of Cars by means of time-dependent density functional theory (TDDFT). We highlight new studies on the charge-transfer state of the Car, peridinin (Per), which enhances the light-harvesting efficiency of the Car by increasing the electronic coupling to Chl. The role of another Car, zeaxanthin (Zea), is discussed with respect to its role in the mechanism of the feedback deexcitation quenching in green plants, a vital regulation process under light conditions which exceed photosynthetic capacity. Lastly, we provide insight on how the 96 Chls in Photosystem I are optimized to generate a pigment-protein complex which utilizes solar energy with near unit efficiency.

Keywords: carotenoid–chlorophyll complexes; light harvesting; feedback deexcitation quenching in green plants; mechanism of energy transfer; dependent density functional theory.

INTRODUCTION

The architecture of photosynthetic light-harvesting complexes (LHCs) has been optimized to achieve the following characteristics: cover the solar spectrum effectively; transmit excitation to the reaction center with near unit efficiency; protect the photosynthetic apparatus against photochemical damage; spatially separate energy and electron transfer; and, in Photosystem II (PS) of green plants and algae, regulate the efficiency of light harvesting. In this article, we will discuss work from our group directed at the elucidation of the biophysical mechanisms that are fundamental to each of the specific design principles. It is remarkable that only two general classes of molecular species, chlorophylls (Chls) and carotenoids (Cars) are used by natural systems to carry out this range of functions. Nature has been rather parsimonious with the types of molecules used in light harvesting, choosing instead to modify their properties by interchromophore and chromophore–protein interactions. Cars have an especially wide range of functions in light harvesting, and in this article, we examine the relationship between the electronic structure of Cars and their function in a variety of light-harvesting systems (Fig. 1). In addition, using Photosystem I (PSI) as an example, we will provide a detailed description of how bacteriochlorophyll (BChl)/Chl interactions generate highly efficient photosynthetic antennas.

---

*Paper based on the acceptance lecture for the 2004 Porter Medal, presented at the XXth IUPAC Symposium on Photochemistry, 17–22 July 2004, Granada, Spain. Other presentations are published in this issue, pp. 925–1085.

†The authors contributed equally to this work.

‡Corresponding author

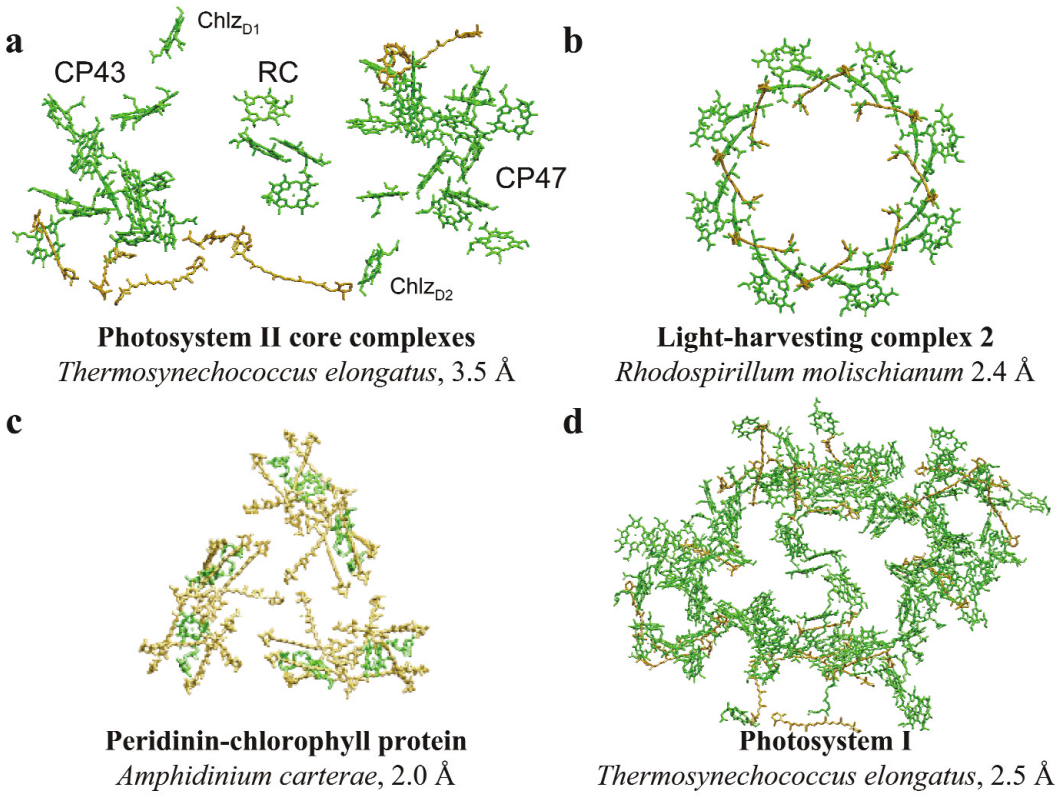

Fig. 1 The arrangement of Chl (green) and Car (orange) pigments in various photosynthetic complexes. (a) PSII from *Thermosynechococcus elongatus* [18]. (b) Light-harvesting complex 2 from *Rhodospirillum molischianum* [29]. (c) PCP from *Amphidinium carterae* [39]. (d) PSI from *Thermosynechococcus elongatus* [75].

LIGHT HARVESTING BY CAROTENOIDS

Solar coverage in the blue/green region, photoprotection, and the regulation of light-harvesting efficiency in PSII are all functions carried out by Car molecules (Fig. 2). The electronic structure of Cars, essentially substituted conjugated polyenes, is rather unusual. They have at least two singlet excited states in the visible region of the spectrum (Fig. 3). One state is the optically allowed S_2 ($^1B_u^+$) state, which absorbs light in the blue/green (~420–510 nm) portion of the spectrum, a region where BChl/Chl has little to no absorption. The other state, S_1 ($^1A_g^-$), is optically dark. Under natural sunlight conditions, the S_1 state is populated by internal conversion from the S_2 state on a timescale of 100–200 fs [1]. Calculation of the electronic structure of Cars is extremely challenging because there is a major contribution from electron correlation. The difficulty of electronic structure calculations from first principles and the short lifetime of the optically prepared S_2 state have led to considerable debate and a certain amount of controversy about the putative existence of one or more additional excited singlet states lying between S_2 and S_1 [2–8].

The first and second singlet excited states of BChl/Chl, Q_y, and Q_x, respectively, accept energy from Cars. While a number of studies on different LHCs agree that the dominant portion of the energy transfer to Chls via Cars proceeds from the Car S_2 state [7,9–12], a role for the Car S_1 state in light harvesting has also been observed and is generally utilized in proteins which have an overall Car to Chl energy-transfer efficiency in excess of ~60 % [7,9,10,13]. Since the Car S_0–S_1 transition is forbidden, the mechanism of S_1 to Chl energy transfer (Fig. 3) is not readily apparent. In this section, we will ex-

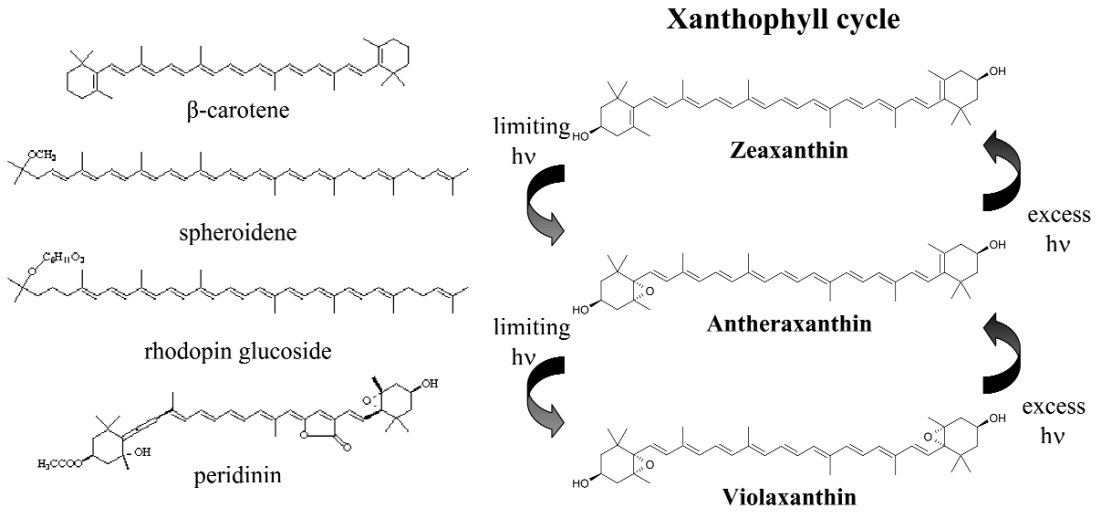

Fig. 2 Molecular structures of the various Cars discussed in this paper.

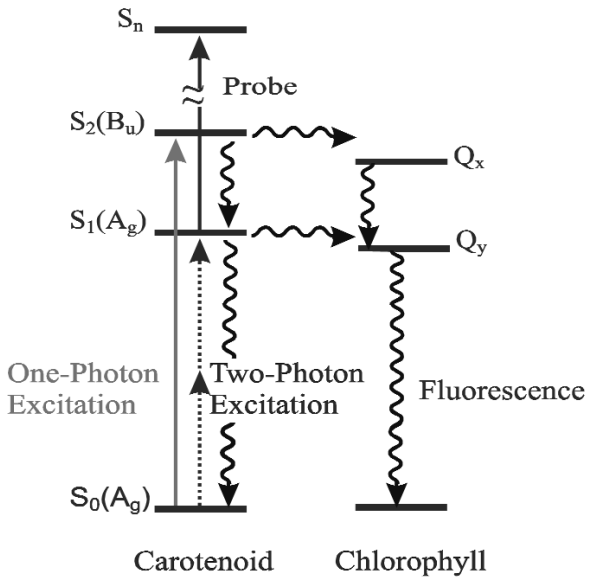

Fig. 3 The energy levels, excitation, probing, and relaxation steps for Car–Chl interactions.

amine the degree of involvement and the mechanism of the energy transfer to Chl for the different Car excited electronic states in a variety of pigment-protein complexes.

PSII CORE PROTEINS

The PSII core is comprised of four pigment binding proteins, CP43, CP47, D1, and D2, all of which have the ability to harvest light (Fig. 1a). CP43 and CP47 (encoded by the psbD and psbC genes, respectively) are relatively similar proteins located adjacent to the PSII reaction center (RC) [14]. Both have a dual light-harvesting role, absorbing energy directly and transferring energy absorbed by the peripheral light-harvesting antenna, which includes light-harvesting complex II (LHCII), CP24, CP26, and CP29, to the RC. Both CP43 and CP47 bind approximately 2 β-carotene molecules and 15 Chls *a*

[15–18]. The Cars in CP47 are believed to be all-*trans* [15–20], however, no complementary information is available for CP43. The D1 and D2 subunits (products of the psbA and psbB genes, respectively) along with cytochrome b559 (encoded by psbE and psbF), PsbI and PsbW, comprise the PSII-RC complex [21–23]. D1 and D2 bind the reaction center pigments, 4-6 Chls *a*, 2 pheophytins, and 2 quinones, which are responsible for charge separation [17,18,21,24]. The PSII-RC also binds 2 β-carotenes which have 0–0 transitions that absorb at 490 and 506 nm and lie out of and in to the membrane plane, respectively. It has been suggested that the two Cars are excitonically coupled [25,26]. It is generally accepted that at least one of the two Cars adopts the all-*trans* conformation.

The decay kinetics of each of the core Chl proteins, excited at 490 nm and detected at 560 nm, and their corresponding single exponential fits are shown in Fig. 4. The value of the S_2 lifetime obtained from these fits was 100 fs (CP47), 97 fs (CP43), 106 fs (PSII-RC), and 62 fs (PSI), each with an error of ±10 fs. Chl fluorescence traces for each of the core complexes, measured with the same excitation wavelength, showed a rise component in the Chl *a* fluorescence, which accounted for either the full rising amplitude or a major component of it, that matched the lifetime of the decay of the Car S_2 state. The findings indicate that the shortening of the lifetime measured for β-carotene in the complexes with respect to solution was due to energy transfer to Chl.

From the measured values of the Car S_2 lifetime, τ_{S2}, we can estimate the lifetime and efficiency of energy transfer from the β-carotene S_2 state to Chl *a* in each of the core complexes. Assuming that the value obtained for the S_2 lifetime in toluene (144 fs) correctly characterizes τ_{IC} in CP47, CP43, and the PSII-RC [27,28], we find that for both CP43 and CP47 τ_{ET} = ~300 fs and φ_{S2} = ~31 %, and for the PSII-RC, τ_{ET} = ~400 fs and φ_{S2} = ~26 %. By combining previous steady-state fluorescence excitation measurements at 77 K, which found that the overall Car to Chl energy transfer for CP43 and CP47 was ~35 % and for the PSII-RC was ~30 %, with our ultrafast results on the Car S_2 lifetime and Chl rise kinetics, we conclude that the β-carotene S_1 state does not play a significant light-harvesting role in the PSII core proteins.

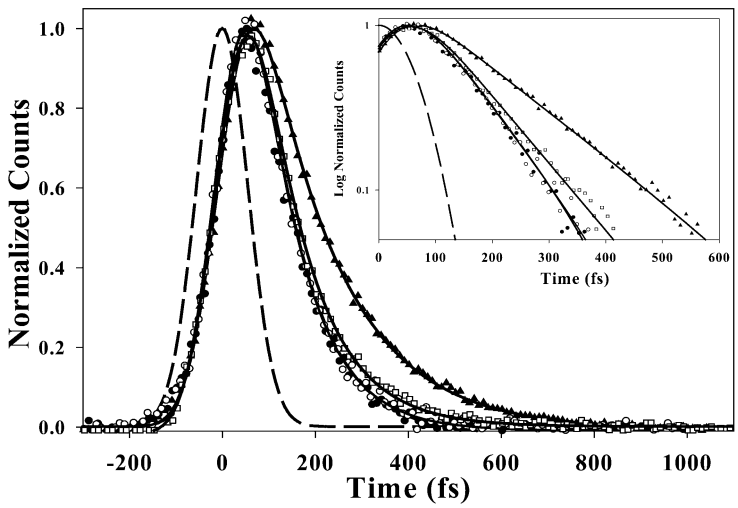

Fig. 4 Normalized experimental upconversion traces and their corresponding single exponential fits (solid lines) for β-carotene in, from left to right: CP43 (open circles), CP47 (solid circles), PSII-RC (open squares), and in *n*-hexane (solid triangles). Insert shows the same data with the counts on a logarithmic scale. A Gaussian IRF of 130 fs is also shown (dashed line). The CP43 and CP47 fits are barely distinguishable even in the logarithmic plot.

LH2

LH2 has two rings of BChls that absorb at 800 (B800) and 850 (B850) nm [29,30] (Fig. 1b). There is also a minor absorption by Cars between 450 and 550 nm. The structure of LH2 from *Rps. acidophila* was determined at 2.5 Å resolution [30]. The complex has 9 BChls in the B800 ring, 18 BChls in the B850 ring, and 9 Cars, which in this structure are rhodopin glucoside.

In designing a photosynthetic antenna, it seems counterintuitive to choose chromophores that have a low-lying excited state that completely lacks a transition dipole moment. However, nature has found an effective way to utilize such states for light harvesting. Energy transfer from the Car S_2 to BChl/Chl in *Rps. acidophila* is extremely rapid (50–100 fs) [31,32], however, the overall efficiency of energy transfer from the Car to BChl is higher than can be explained by the Car S_2 transfer pathway alone. An alternate pathway via S_1 is involved (Fig. 3) [7]. In order to unequivocally prove that there is S_1 to BChl/Chl energy transfer in photosynthetic antenna, we developed various forms of two-photon excited ultrafast spectroscopy, which prepared the S_1 state directly from the ground state (i.e., not by S_2 internal conversion, as was done previously) [10,33,34]. We found the S_1 to BChl energy-transfer timescale in bacterial LH2 from *Rb. sphaeroides* to be ~3 ps [10] and determined the spectrum and dynamics of Car S_1 (Fig. 5).

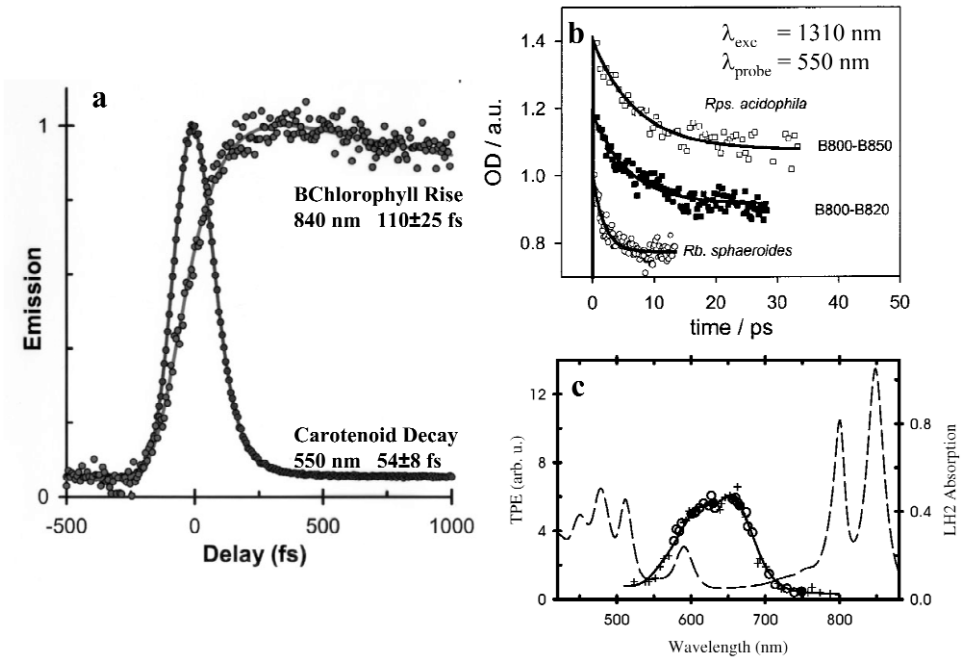

Fig. 5 (a) Fluorescence upconversion data showing the decay of Car (rhodopin glucoside) S_2 fluorescence and the rise of BChl fluorescence in LH2 of *Rps. acidophila*. (b) Time dependence of excited-state absorption of the B800-B850 complex (open squares, $\tau_{S1} = 7 \pm 0.5$ ps), the B800-B820 complex (solid squares, $\tau_{S1} = 6 \pm 0.5$ ps) of *Rps. acidophila*, and LH2 of *Rb. sphaeroides* (open circles, $\tau_{S1} = 1.9 \pm 0.5$ ps) observed after TPE of the S_1 state. The traces have been normalized and offset from each other by 0.2. (c) Two-photon fluorescence excitation spectrum (solid line) and one-photon absorption spectrum (dotted line) of LH2 from *Rb. sphaeroides* strain 2.4.1.

The involvement of the S_1 state in light-harvesting highlights a spectacular failure of the dipole model in characterizing photosynthetic pigment interactions: since S_0–S_1 has a very small net transition dipole moment because the photon averages over the entire molecule, the calculated rate would be zero. However, the Coulomb interaction between two regions of transition density, *i* and *j*, is given by

($q_i q_j / r_{ij}$). Therefore, the overall Coulombic coupling, which is the sum of the interactions between all such elements, depends on the full shape of the donor and acceptor transition density on a length scale much smaller than the molecular size. As a result, we developed a highly accurate method, called the transition density cube (TDC) method, to calculate the full Coulombic coupling between two molecules [35]. In short, this is done by dividing the transition densities of the states involved into small cubes and computing the coupling by summing over all of the cube–cube interactions (Fig. 6). TDC combined with time-dependent density functional theory (TDDFT) [36] gives values of the full Coulombic S_1-BChl coupling that are in excellent agreement with experimental estimates [37]. When incorporated into a generalized Förster theory model, the calculated energy-transfer rates both agree with experiment and quantitatively account for the large difference in S_1 to BChl transfer efficiency in the LH2 complexes of *Rps. acidophila*, *Rs. molischianum*, and *Rb. sphaeroides* [10,37] (Fig. 5). Furthermore, we showed that when the LH2 structure is modeled with a strictly symmetric polyene whose transition dipole is rigorously zero, sizeable Coulomb coupling to BChl can still occur simply from spatial proximity and the asymmetric arrangement of donors and acceptors [37].

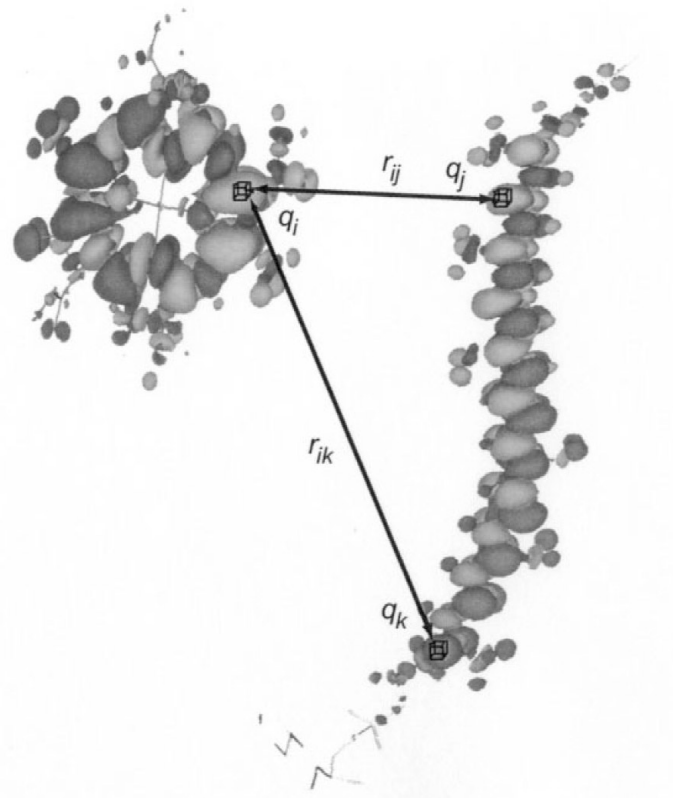

Fig. 6 Transition densities calculated for a BChl molecule and a Car. Density elements, containing charges q_i and q_j, are depicted together with their corresponding separation r_{ij}.

As an aside, we note that singlet–singlet energy transfer involving transitions with little or no oscillator strength is often discussed in the context of electron-exchange interactions between donor and acceptor—the Dexter mechanism [38]. While this form of coupling is undoubtedly crucial in triplet–triplet transfers, in all of the singlet–singlet transfer cases we have examined, the Coulombic coupling is much larger than the exchange coupling and the energy transfer is fully describable with Coulombic coupling alone.

PCP

Peridinin is a Car found in the light-harvesting apparatus of dinoflagellates, called peridinin-Chl *a*-protein (PCP) [39]. In contrast to most photosynthetic LHCs, the Car peridinin (Per), and not the Chl, is the main light-absorbing pigment in PCP (Fig. 1c). Per is an unusual Car, being the only one known with three full rings in its structure (Fig. 2). Furthermore, it contains an allene group, an epoxy group, and two carbonyl groups, including a lactone ring. Previous studies have shown that Per's unique structure significantly alters the character of its excited states. In addition to the usual S_1 and S_2 states, strong evidence has emerged for the existence of a low-lying intramolecular charge-transfer (ICT) state in polar environments and in the PCP complex [40–43]. After light absorption by Per, the excitation energy is transferred to Chl and the efficiency of this energy-transfer step is 88 % [11]. Previous studies have suggested that the majority of the energy is transferred through Per's S_1 state [44]. However, fluorescence upconversion studies suggest that ~50 % of the overall transfer occurs from the Per S_2 state (Fig. 7a). Involvement of the ICT state in energy transfer has also been proposed [45].

Transient absorption studies were the first to display the spectroscopic peculiarities of Per [40,41]. The S_1 lifetime was found to be strongly dependent on solvent polarity: 7 ps in trifluoroethanol and 172 ps in cyclohexane. From these studies, Frank et al. concluded that the presence of the carbonyl group as part of the conjugated π-electron system is the source of the solvent dependence. To map out the Per S_0–S_1 line shape, we measured the fluorescence excitation spectra after two-photon excitation

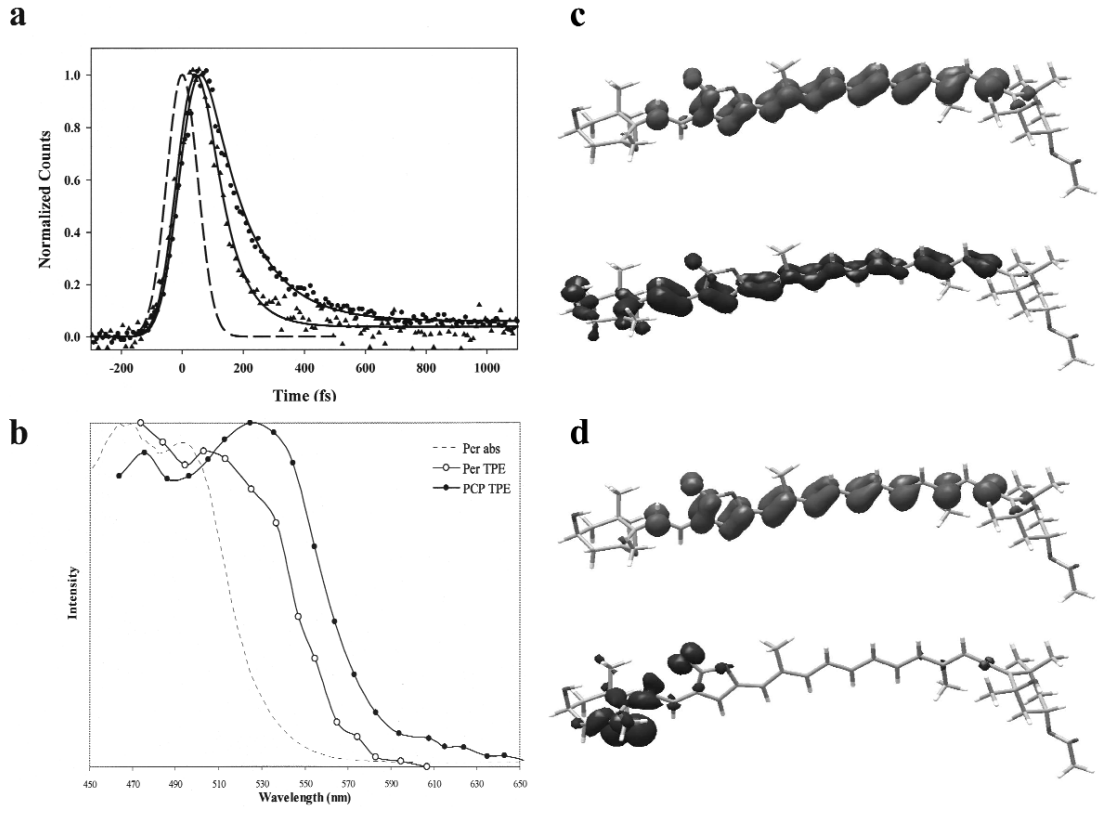

Fig. 7 (a) Fluorescence upconversion data for Per in methanol solution (solid circles) and PCP (solid triangles). The instrument reponse function is shown by the dashed line and best fits to the data by the solid lines. (b) Two-photon fluorescence excitation spectra of Per (open circles) in benzene and in PCP (solid circles). The one-photon absorption spectrum is also shown (dotted line). Attachment (top) and detachment (bottom) density plots of Per 612 from PCP: (c) the S_1 state, (d) the ICT state.

for Per in benzene and PCP (Fig. 7b). The samples were excited using 920–1320 nm light. Fluorescence of the isolated Per S_1 state was then measured at 750 nm for Per in solution. In PCP, the excited Per transfers energy to Chl whose fluorescence was monitored at 670 nm. Surprisingly, two-photon absorption was observed in both the S_1 and S_2 regions. The Per S_1 energy was found to be higher than that of typical light-harvesting Cars, making its S_1 state very close in energy to its S_2 state. Two-photon absorption observed to the red of the one-photon S_2 band is assigned to the S_1 state, since no maximum is observed for this state, the origin of the transition was estimated to be around 530–540 nm in benzene, and 550–560 nm in PCP [46]. Thus, the S_1 state appears strongly overlapped with S_2, and it does not seem possible to extract an S_1 line-shape from the data in Fig. 7b since the relative S_1 and S_2 contributions are unknown. We suggest that Per's polar groups and the mixing of electronic states lead to two-photon character of the normally one-photon allowed S_0–S_2 transition. Additional two-photon excited pump-probe data on Per in methanol and PCP [47] are consistent with the conclusions of Zimmermann et al. [46] and Shima et al. [48] that a separate two-photon-allowed transition exists just to the red of the strongly allowed S_0–S_2 band. Excitation at 1150 nm clearly prepares a different state than at 1100 nm, most likely the S_1 state.

Two-photon studies of Per, however, could not definitively place the S_1 band, nor were they able to explain the solvent dependence of the S_1 lifetime. TDDFT under the Tamm–Dancoff approximation (TDDFT/TDA) has been quite successful at obtaining Car S_1 and S_2 energies, oscillator strengths, and transition densities [37,49]. The Car–Chl couplings obtained using the calculated transition densities are in excellent agreement with experimental results [37]. TDDFT/TDA studies of Per structurally optimized and in the 8 conformations of PCP give in vacuo (roughly corresponding to *n*-hexane) S_1 energies ranging from 590–620 nm (Table 1). The S_1 attachment/detachment density plots of Per 612 in PCP (nomenclature as per the protein databank file 1PPR [39]) are shown in Fig. 7c. The attachment density approximately cancels the detachment density across the molecule leaving S_1 with an oscillator strength of 0.08.

Table 1 In vacuo excitation energies (λ) and oscillator strengths (f) for the various conformers of Per in PCP.

Per	A_g^-		B_u^+		CT	
	λ (nm)	f	λ (nm)	f	λ (nm)	f
611	610	0.0	521	4.4	538	0.1
612	618	0.1	557	1.1	521	0.4
613	612	0.0	520	4.5	504	0.3
614	619	0.0	528	2.5	507	2.0
621	600	0.0	526	4.2	511	0.7
622	609	0.0	526	4.6	511	0.0
623	606	0.0	527	1.8	506	2.7
624	590	0.0	524	4.2	506	0.5

TDDFT/TDA calculations also provide strong evidence for the existence of an ICT state. In vacuo, the ICT state is calculated to be higher in energy than S_1 and even S_2, but in a polar solvent with a dielectric constant of 33 the ICT state is stabilized by ~8000 cm^{-1} to become the lowest excited state [45]. Attachment/detachment density plots of the Per ICT transition are shown in Fig. 7d. Transition to the ICT state distributes electron density from the carbonyl group to the conjugated chain. The advantage of this is clear when we consider the structure. Figure 8 shows the arrangement of Per and Chl molecules in half of a monomer of PCP. The Chl molecule lies with its center closer to the allene end of Per molecules, away from the lactone ring, therefore, transfer to the ICT state transfers excitation closer to the Chl. For example, in Per 611 the separation of the lactone ring from the Chl Mg atom is 13.0 Å, while the Mg-allene distance is 8.7 Å. The other Per molecules in PCP lie with the allene region even

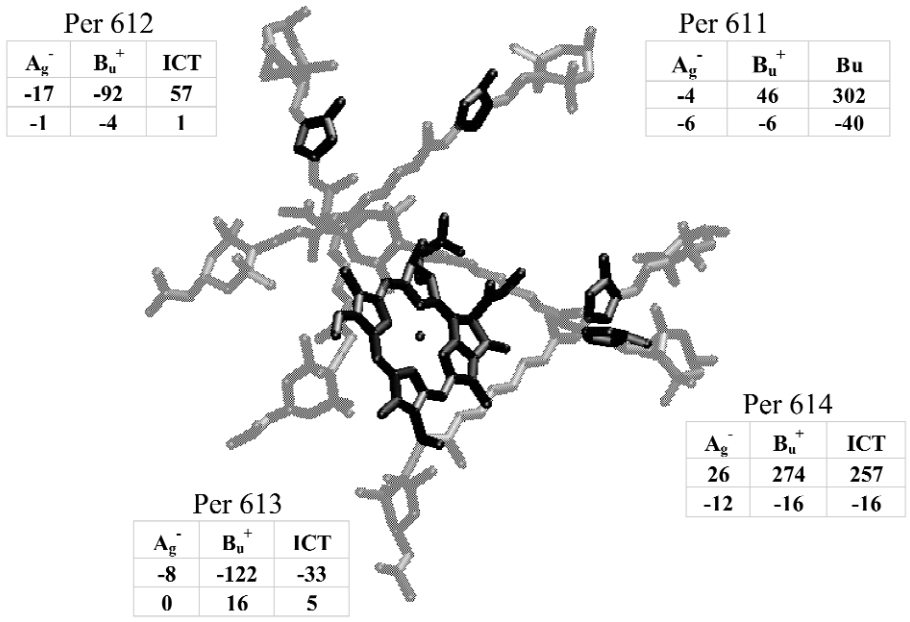

Fig. 8 Geometry of Per (gray) and Chl (black) in half a monomer of PCP. The lactone ring of Per is shown in black. The tables show the coupling strength between the Car A_g^-, ICT, and B_u^+ states and the Chl Q_x (first row) and Q_y (second row) states for each Per.

closer to the Chl, with Mg 4.3 to 7.5 Å from the allene group compared to 9.7 to 14.6 Å from the lactone ring. The Coulombic couplings calculated using the TDC method [35] quantitatively confirm our analysis. The ICT–Chl Q_y couplings are consistently an order of magnitude larger than the A_g–Chl Q_y couplings (Fig 8). We conclude that the role of the ICT state is to facilitate energy transfer to Chl. We note that the MNDO-PSDCI calculations of Shima et al. [48] do not show an additional ICT state. Instead, the S_1 surface is considered to be a double well: one minimum corresponds to the traditional S_1 state and the other to the ICT state. The double-well model gives rise to eventually the same interpretation of the spectroscopic data and also suggests the ICT part of S_1 facilitates energy transfer to Chl. Advances in quantum chemical calculations are required to fully explore the geometry of the excited states of unusual Cars such as Per.

Recent near-infrared (IR) transient absorption (TA) experiments of Per in methanol revealed the spectroscopic signature of an ICT state and explain the solvent dependence of the Per pump-probe and fluorescence data. Specifically, a new stimulated emission band appears at 980 nm, far lower than the S_1 fluorescence peak at 715 nm [42]. The band is only present in carbonyl containing Cars in polar solvents [42,43,50–54], in good agreement with our TDDFT calculations.

PHOTOPROTECTION BY CAROTENOIDS

A green plant's ability to remove electrons from water requires that the PSII-RC has the highest oxidizing potential found in nature. The consequences of this great oxidizing strength have generated unique sensitivities for green plants, with respect to their anoxygenic photosynthetic counterparts, under conditions in which photon fluxes exceed photosynthetic capacity. Specifically, the production of harmful photo-oxidative species, which cause destruction of vital proteins, such as the PSII D1 RC protein, lipid bilayers, and pigments [55,56], is exacerbated during high light exposure. As a result, plants employ a regulatory mechanism, which allows them to both utilize and dissipate solar energy with high efficiency in response to the incident light intensity.

The process which protects plants under most short-term light stress conditions occurs in PSII and is called feedback deexcitation quenching (qE) ([57,58]; for a review of this process, see [59]). During qE, a nonradiative deactivation channel for singlet Chl molecules (^{1}Chl*) has been formed which can harmlessly emit the excess absorbed energy as heat (Fig. 9). The process significantly decreases the probability that the ^{1}Chl* molecules will form triplet Chl molecules (^{3}Chl*), a species that reacts with ground-state oxygen ($^3O_2$) to form the strongly photo-oxidative singlet oxygen ($^1O_2$*) in addition to other highly reactive oxygen species [60]. In green plants and algae, qE can quench up to 80 % of the ^{1}Chl* [61–63]. Three elements are so far known to be necessary for qE. Specifically, the Car zeaxanthin (Zea), which is formed during qE by conversion from violaxanthin (Vio) via reversible reactions known as the xanthophyll (Xan) cycle [64]. The 22-kDa subunit of PSII, PsbS [63], and a low thylakoid lumen pH [57,65] are the other two requirements.

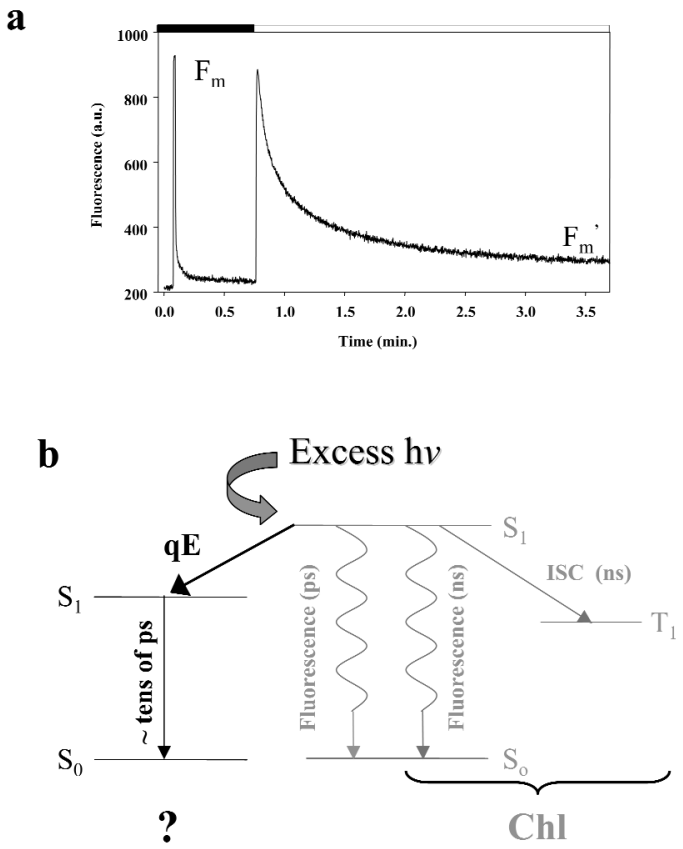

Fig. 9 (a) Chl fluorescence in isolated spinach thylakoid membranes with (black bar above the graph) and without (white bar) continuous, high light illumination. F_0 is the fluorescence with open reaction centers in the absence of high light. F_m and F_m' correspond to the fluorescence with closed reaction centers (achieved with a saturating pulse, ~ 2200 μE, 60 s) in the absence and presence of continuous, high light, respectively. Insert shows F_m' measured ~5 min after quenched TA measurement. (b) Scheme of decay channels [Chl-related states (gray) and the quencher state (black)] for the first singlet excited state of Chl during qE.

The key unresolved issues concerning the mechanism of ^{1}Chl* deexcitation during qE are the identity of the quenching species, in terms of both pigment composition and location, and the means by which the excess energy is dissipated. Based on the strong correlations between qE and Zea in plants, it was suggested that ^{1}Chl* deexcitation might involve direct energy transfer from Chl to Zea [66–68].

As a result of this transfer, Zea would be excited to its first excited singlet state (S_1), which would decay rapidly (~9 ps) to the ground state by nonradiative dissipation. In order for this mechanism to be efficient, the energy of the S_1 state of Zea must lie below the state corresponding to ^{1}Chl* (Q_y). Since the S_1 states of Cars are, for all intents and purposes, optically dark, obtaining an accurate value for the energy of this state has proven to be a formidable task. While there is no general consensus on the energy of the Zea S_1 state, a number of measurements suggest that its energy is comparable to the value of the Chl Q_y band [50,68–70]. Alternatively, ^{1}Chl* deexcitation may be due to an increased rate of internal conversion of Chl to the ground state by the formation of an exclusively Chl-based quenching species, a process which would be indirectly enhanced by the presence of Zea [65,71] .

In order to gain further insight into the quenching mechanism, we performed TA measurements on intact thylakoid membranes with fully functional qE capability [72]. The measurements probed changes in the region of the Car $S_1 \rightarrow S_n$ transition after excitation of the Chl Q_y band. Kinetic differences were evaluated when the system had no qE and when maximum, steady-state qE had been induced. The results for spinach reveal an additional transient component with the lifetime and spectral characteristics of Zea $S_1 \rightarrow S_n$ absorption selectively under conditions of qE.

To test if the changes were correlated to qE, we performed additional experiments on transgenic *A. thaliana* plants, two completely deficient and one enhanced in qE with respect to the wild type (WT), but all normal in their ability to carry out direct light-induced photochemistry (Fig. 10). The *WT + PsbS* mutant displays approximately 2.5 times more qE than the WT [58], and the amplitude of the new kinetic component is increased by roughly this amount compared to the WT. Figure 10c show the results for the completely qE-deficient mutant *npq4-1*. The kinetics observed for the *npq4-1* mutant was independent of high-light illumination, showing that fully functional qE is required for the observation of the new transient. Additional experiments on *A. thaliana* mutants with distinct Car compositions showed that Zea is also necessary to produce the ultrafast kinetic differences.

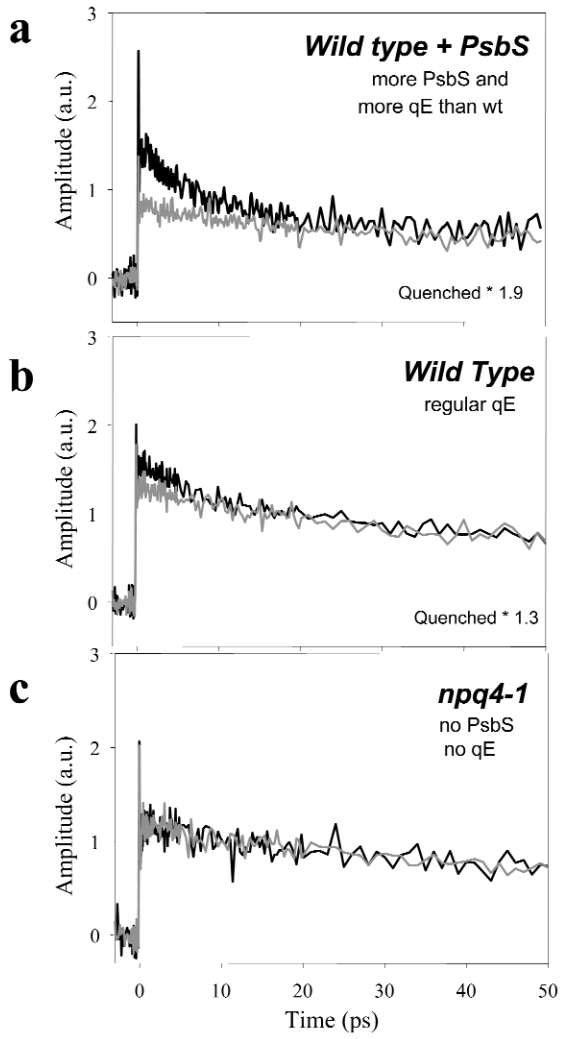

Fig. 10 The scaled TA kinetics measured at 540 nm upon excitation at 664 nm for *A. thaliana* plants: (a) *WT* + *PsbS*, (b) *WT*, and (c) *npq4-1*. The gray and black lines indicate maximum, steady-state, and no qE conditions, respectively, for the samples with qE capability, which corresponds to ON and OFF, respectively, for high light illumination in the qE deficient mutants. The decay profiles were normalized to 1.0 at the maximum amplitude of the no qE (light OFF) kinetics.

By using the mutants and transgenic plants described above, we were able to identify a PsbS- and Zea-dependent kinetic difference in TA during qE [72]. The Zea excited state may be populated via energy transfer from the Chl Q_y band or by the formation of a Zea-Chl heterodimer, the more likely possibility because of the characteristics of the kinetic difference. The heterodimer species may be the qE quencher. Furthermore, the formation of a heterodimer during qE may imply an electron transfer quenching mechanism. Recent calculations by Dreuw et al. [73,74] using a hybrid theoretical approach involving TDDFT and configuration interaction singles, indicate that two Chl Q_y quenching mechanisms are energetically accessible. Since the S_1 state of Zea is lower in energy than the Q_y state of Chl independent of the intermolecular distance, excitation energy transfer is in principle always possible and dimer formation is not a prerequisite for this mechanism. When the intermolecular separation is less than 5.5 Å (where the CT curve crosses Q_y in Fig. 11), the energy of the CT state drops below that of

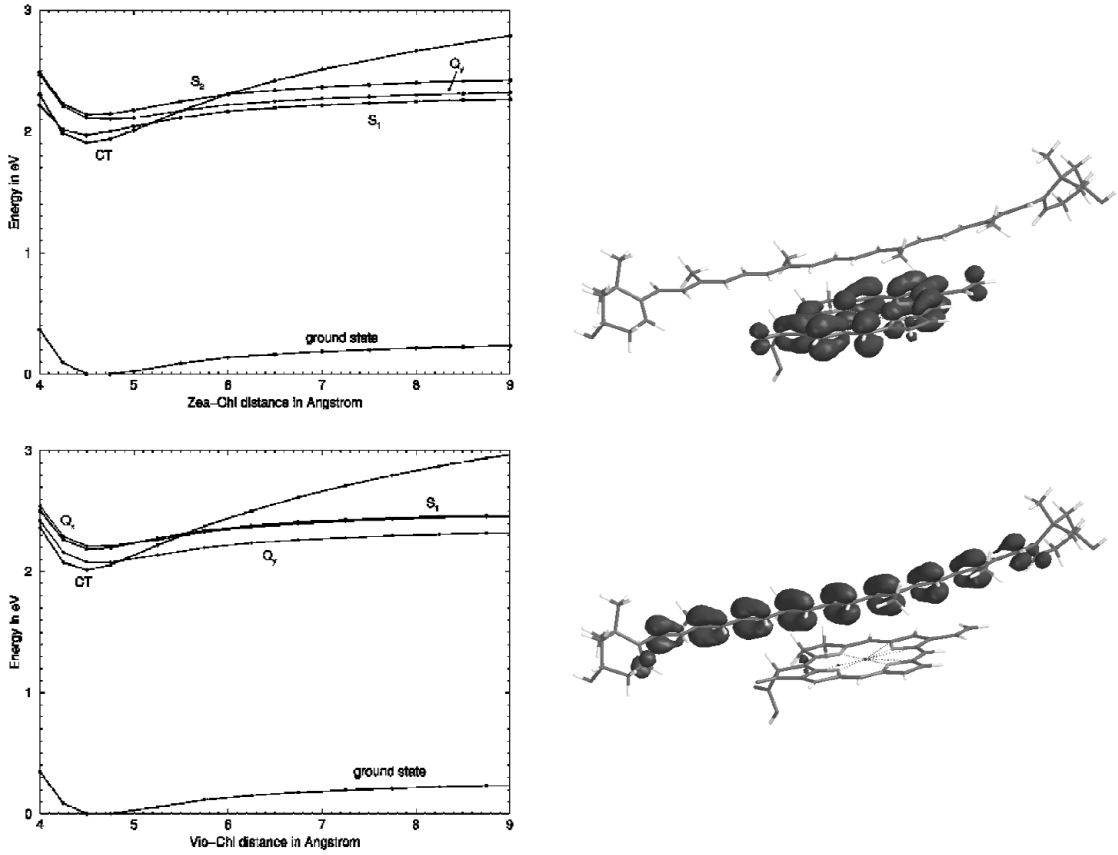

Fig. 11 Potential energy surfaces of the ground and excited states of the Zea-Chl dimer (upper left) and the Vio-Chl dimer (lower left) along the distance coordinate between the Car and Chl. HOMO (lower right) and LUMO (upper right) of the Zea-Chl dimer. The energetically lowest CT state corresponds to a pure HOMO–LUMO transition.

Chl Q_y. Consequently, a second quenching pathway, via electron transfer, becomes possible. Analysis of the molecular orbitals involved in this excited CT state shows that it is a pure HOMO (highest occupied molecular orbital) to LUMO (lowest unoccupied molecular orbital) transition (Fig. 11). Similar calculations for Vio show that the excitation energy of the S_1 state (dashed curve) is significantly higher than the Chl Q_y at all intermolecular distances. Consequently, Chl fluorescence quenching via singlet–singlet excitation energy transfer into the S_1 state is energetically not possible at all intermolecular distances. The electron-transfer quenching mechanism only becomes possible at intermolecular separations of less than 4.8 Å [73].

While the mechanism of qE is still unclear, these TA measurements and theoretical calculations may provide another case in which nature has utilized optically dark states and confined geometries as a means to a very efficient end.

LIGHT HARVESTING BY CHLOROPHYLL: PSI

Photosystem I from *Thermosynechococcus elongatus* comprises 96 nonequivalent Chls (Fig. 1d) [75]. In a system like PSI with large variation in Chl site energies, understanding the principles, dynamics, and pathways of Chl–Chl energy transfer is demanding. We tackled this problem by asking the following questions: Are there new design principles at work in PSI? How is the system optimized to focus

and trap excitation at the primary electron donor (P700)? What are the rate-determining steps? And is a first-principles calculation viable for quantitative predictions on such a complex system? [76–79].

Calculations from first principles are challenging because of the presence of both moderately or strongly coupled pigments and pigments spaced at distances that make a weak coupling picture inappropriate. For these types of calculations, modified Redfield theory was utilized [80,81]. We first calculated the excitation energies of and couplings between each of the 96 Chls in the protein environment and obtained a good fit to the absorption spectrum [79]. Unlike bacterial light-harvesting antennas, PSI does not appear to have an energetic funnel, i.e., the outermost pigments do not, on average, have higher excitation energies than the pigments in the reaction center.

We used our calculated excitation energies, modified Redfield theory, and a master equation calculation of the excitation transfer kinetics in PSI to calculate time-dependent fluorescence spectra and population kinetics. We found that the time constants are clustered into four groups: sub-100 fs, 200–300 fs, 2–3 ps, and 35–40 ps [77]. The global fits to experimental fluorescence data gave time constants of 360 fs, 3.6 ps, 9.6 ps, and 38 ps [13]. The experiments did not have sufficient time resolution to determine sub-100 fs time constants. Aside from this, our calculated time constants were in remarkable agreement with experimental values (Fig. 12).

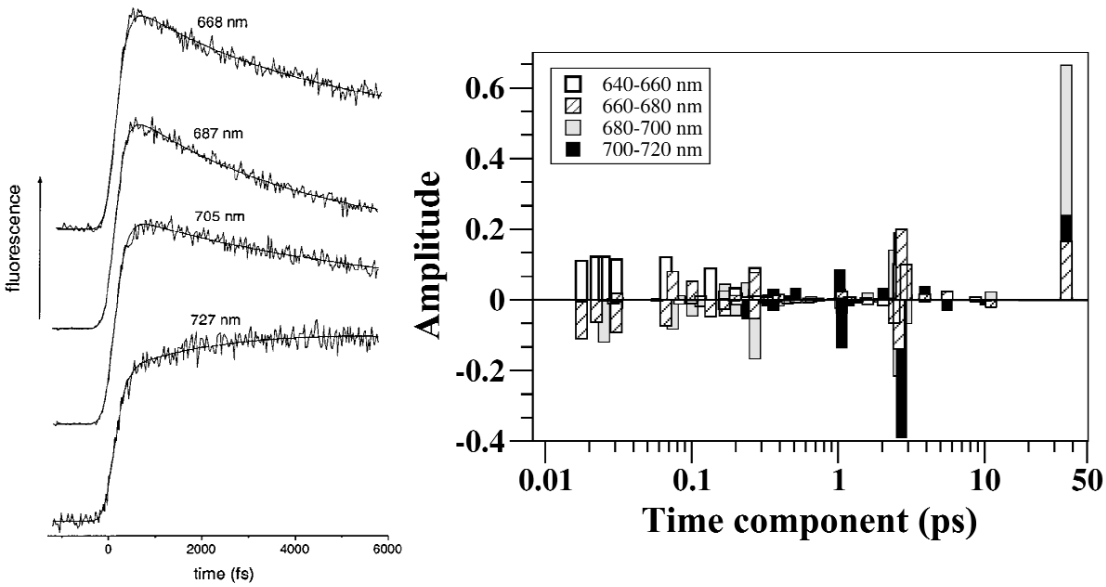

Fig. 12 Wavelength-dependent fluorescence upconversion data for PSI (left). Distribution of the calculated time components of fluorescence decay at three different detection windows after excitation at 640–660 nm (right). Positive amplitudes correspond to decays, negative amplitudes to rises.

Having developed a model of PSI that reproduced key experimental data, we explored the influence of the energy landscape [76,77] on the trapping time and performed a detailed analysis of the rate-determining steps [78]. In a flat energy landscape, where all the Chls had identical lineshapes and transition energies, and the spatial structure was held fixed, the calculated trapping time of PSI was actually shorter. However, due to protein constraints and the proximity of the chromophores (which induces excitonic interactions), a flat energy landscape cannot be achieved in a realistic PSI complex. The high spatial connectivity of PSI makes it very robust to energy variation, however, the energies of the six RC Chls influence the overall trapping time significantly. Along with the two linker Chls, the six RC Chls form a quasi-funnel structure: the energies of the RC and linker Chls are optimized for efficient trans-

fer of excitation to the P700; although, the precise energies of the other 88 antenna pigments are not crucial to the near unit quantum efficiency of PSI [77].

Studies of the energy distribution in PSI after initial excitation of two different Chl molecules show that energy flow through the antenna contributes significantly to the overall trapping time [76]. We developed a formulation allowing construction of uniquely defined kinetic domains from a master equation for population-transfer dynamics and enabling calculation of the time scales of transition between such domains [78]. In this way, the complicated network of energy-transfer steps in PSI can be simplified to a series of sequential kinetic transitions over the kinetic domains. Five innermost kinetic domains for PSI are presented in Fig. 13. The overall trapping time is 36 ps, which should be a sum of

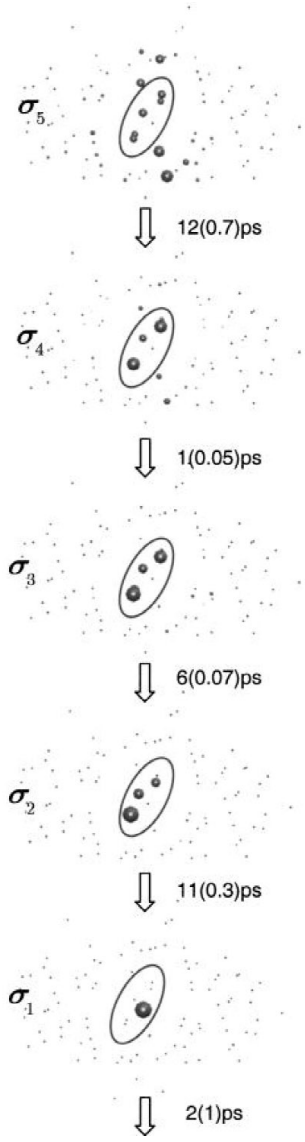

Fig. 13 Configurations of the five innermost kinetic domains of PSI. The locations of the 96 Chl molecules are marked as tiny spots, and the participation of a Chl in each kinetic domain is proportional to the surface area of the sphere sitting on the Chl. For clarity, the six RC Chls are encircled by an ellipsoid at the center of the complex. The effective transfer times toward the inner domains are shown along with the direct inward transfer times given in parenthesis.

the 96 effective transfer timescales. We can see that there are two major rate-determining steps: transfer from domain σ_5 to domain σ_4 (12 ps) and from domain σ_2 to the trap σ_1 (11 ps). The next slowest step is the transfer from domain σ_3 to domain σ_2 (6 ps). These three steps make up 81 % of the total trapping time, and the other 93 steps make up the remaining 19 %. The domain model reveals that back transfer, including components from the RC Chls to the bulk antenna, contributes substantially to the overall trapping time, indicating that energy transfer around the RC is dominated by entropic rather than enthalpic considerations.

The complexity of the system, and therefore of any microscopically based model, suggests that experiments either with higher information content, or designed to reveal specific features of the system should be considered for PSI. For example, the three pulse photon echo peak shift spectroscopy (3PEPS) [82,83] can be used to test the model and experimentally study the pathways of excitation in PSI. 3PEPS is an incisive tool in the study of energetically disordered systems, exploiting the disorder to determine energy-transfer timescales, electron–phonon coupling, and the degree to which the disorder is correlated within individual complexes. Our group has recently developed a two-dimensional extension of traditional 3PEPS, two-color 3PEPS (2C3PEPS) [84–87], to determine electronic mixing between pairs of excitonically coupled molecules, without prior knowledge of the uncoupled site energies. Details of the experimental method, information content, and analysis procedures are given elsewhere [84,85]. This new technique provides previously unmeasurable information about the degree of correlation and excitonic coupling between the initial and final states. Two-color 3PEPS experiments were conducted on PSI with the first two pulses at 675 nm and the third at 690 or 700 nm. These measurements are characterized by a quantity called the difference peak shift (DPS). A rapid, almost instantaneous, rise to a large DPS is measured (Fig. 14a), suggesting large correlation between pump and probe regions. This DPS decays on the timescale of hundreds of femtoseconds. The DPS calculated from the inhomogeneous contribution to the averaged frequency correlation function, I(t), provided by the calculations fit reasonably with the experimental results (Fig. 14b). If we use Förster theory instead of modified Redfield theory, I(t) decays more slowly suggesting that ultrafast relaxation between states of individual excitons contribute significantly to the short-time behavior of the DPS. In an artificially flat energy landscape, where all but the Chl trap have the same site energy and lineshape, I(t) decays more rapidly, revealing the influence of the rough energy landscape. We compute I(t) for various permutations of the quantum mechanical site energies and for random orientations of the pigments. The results show that 2C3PEPS is sensitive to both the exact distribution of energies (not just the gross distribution) and the coupling generated by the crystal structure orientations (data not shown).

In summary, the transfer of excitation to P700 of PSI is an exceedingly efficient process. Overall, it differs markedly from the same process in the well-studied purple bacteria [88,89]. While the two-dimensional projection of PSI (Fig. 1d) seems to imply that the isolation of the antenna from the electron-transfer components is the same as in purple bacteria (RC1 + LH1), this is an incorrect picture. Three important comparisons between the two systems illustrate the differing design principles in the two systems. PSI is quasi-three-dimensional, whereas RC/LH1 is quasi-one-dimensional; all six members of the RC Chls are energetically accessible from the antenna system in PSI, whereas only the primary electron donor is accessible in purple bacteria; and only PSI has linker Chls, which play a role in connecting the reaction center pigments to the bulk antenna, facilitating both forward (to the RC) and reverse (to the antenna) energy flow. These two systems efficiently solve the same problem in two different ways by exploiting the confined geometry and spatial and energetic disorder.

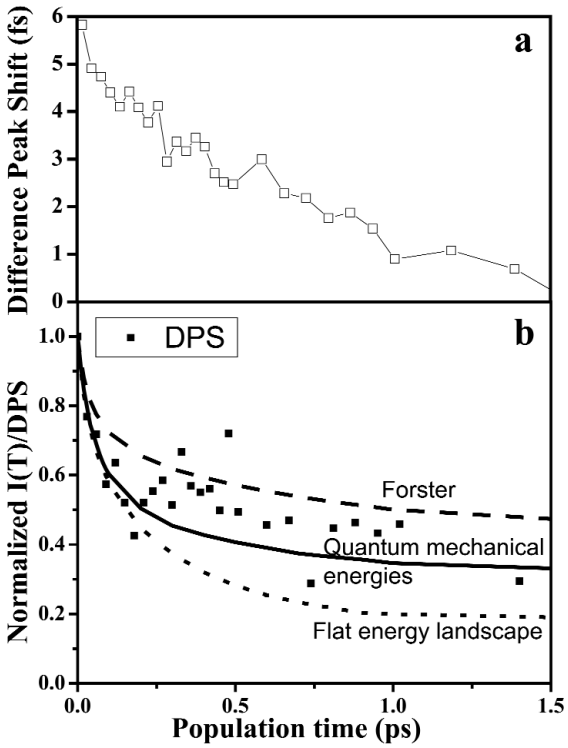

Fig. 14 Two-color 3PEPS data obtained for PSI. (a) Difference peak shift (DPS). (b) Normalized DPS and the inhomogeneous contribution to the electronic frequency correlation function, I(t), for the quantum mechanical energies using modified Redfield theory (solid line) and Förster theory (dashed line). The dotted line shows I(t) (using modified Redfield theory) in a flat energy landscape.

CONCLUDING REMARKS

In this article, we have surveyed the roles of Cars in plant, algal, and bacterial light-harvesting systems, and described the insights gained from a first-principles study of energy transfer and trapping in PSI. Several general concepts emerge: confined molecular geometries are used very frequently to modify molecular properties, introduce new electronic states, ensure effective electronic couplings, and provide very large absorption cross sections for solar radiation. In many ways, this theme contrasts with synthetic chemical approaches based on theories and concepts obtained for well-separated molecular pairs. We have discussed the fundamental inadequacy of linear optical spectroscopic measurements of the intermolecular interactions in such crowded geometries elsewhere [90,91], and newly emerging multidimensional spectroscopic methods [92,93] should begin to provide experimental insight into molecular interactions in the next few years. This is important because at present quantum chemical calculations are necessary to create first-principles models of these systems, yet such calculations are at, and sometimes beyond, the capability of correct computational methods. Thus, experimental feedback is required to calibrate existing methods (such as TDDFT [36]) and to validate newly emerging methods such as the quantum Monte Carlo technique [94–97]. The creation of a first-principles model for PSII, nature's supreme example of photonic engineering, is not yet possible because of the extraordinary complexity, and the lack of atomic-resolution structural data for the complex. Achieving such a goal is likely to drive developments in electronic structure theory, multidimensional spectroscopy, and structural biology for many years to come.

ACKNOWLEDGMENTS

This work was supported by the Director, Office of Science, Office of Basic Energy Sciences, Chemical Sciences Division, of the U.S. Department of Energy under contract number DE-AC03-76SF00098. We thank the many members of the Fleming group whose contributions are described here.

REFERENCES

1. A. N. Macpherson and T. Gillbro. *J. Phys. Chem. A* **102**, 5049–5058 (1998).
2. T. Ritz, A. Damjanovic, K. Schulten, J. Zhang, Y. Koyama. *Photosynth. Res.* **66**, 125 (2001).
3. T. Sashima, H. Nagae, M. Kuki, Y. Koyama. *Chem. Phys. Lett.* **299**, 187–194 (1999).
4. T. Sashima and Y. Koyama. *J. Phys. Chem. B* **104**, 5011–5019 (2000).
5. E. Papagiannakis, J. T. M. Kennis, I. H. M. van Stokkum, R. J. Cogdell, R. van Grondelle. *Proc. Natl. Acad. Sci. USA* **99**, 6017–6022 (2002).
6. G. Cerullo, D. Polli, G. Lanzani, S. De Silvestri, H. Hashimoto, R. J. Cogdell. *Science* **298**, 2395–2398 (2002).
7. J. P. Zhang, R. Fujii, P. Qian, T. Inaba, T. Mizoguchi, Y. Koyama, K. Onaka, Y. Watanabe, H. Nagae. *J. Phys. Chem. B* **104**, 3683–3691 (2000).
8. R. Fujii, T. Fujino, T. Inaba, H. Nagae, Y. Koyama. *Chem. Phys. Lett.* **384**, 9 (2004).
9. C. C. Gradinaru, I. H. M. van Stokkum, A. A. Pascal, R. van Grondelle, H. van Amerongen. *J. Phys. Chem. B* **104**, 9330–9342 (2000).
10. P. J. Walla, P. A. Linden, C.-P. Hsu, G. D. Scholes, G. R. Fleming. *Proc. Natl. Acad. Sci. USA* **97**, 10808–10813 (2000).
11. B. P. Krueger, S. S. Lampoura, I. H. M. van Stokkum, E. Papagiannakis, J. M. Salverda, C. C. Gradinaru, D. Rutkauskas, R. G. Hiller, R. van Grondelle. *Biophys. J.* **80**, 2843–2855 (2001).
12. R. Croce, M. G. Müller, S. Caffarri, R. Bassi, A. R. Holzwarth. *Biophys. J.* **84**, 2517–2532 (2003).
13. J. T. M. Kennis, B. Gobets, I. H. M. van Stokkum, J. P. Dekker, R. van Grondelle, G. R. Fleming. *J. Phys. Chem. B* **105**, 4485–4494 (2001).
14. T. M. Bricker. *Photosynth. Res.* **24**, 1–3 (1990).
15. X.-S. Tang and K. Satoh. *Plant Cell Physiol.* **25**, 935–945 (1984).
16. R. Barbato, H. L. Race, G. Friso, J. Barber. *FEBS Lett.* **286**, 86–90 (1991).
17. A. Zouni, H. T. Witt, J. Kern, P. Fromme, N. Krauss, W. Saenger, P. Orth. *Nature* **409**, 739–743 (2001).
18. K. N. Ferreira, T. M. Iverson, K. Maghlaoui, J. Barber, S. Iwata. *Science* **303**, 1831–1838 (2004).
19. J. C. de Paula, A. Liefshitz, S. Hinsley, W. Lin, V. Chopra, K. Long, S. A. Williams, S. Betts, C. F. Yocum. *Biochemistry* **33** (1994).
20. B. Hankamer, J. Barber, E. J. Boekema. *Annu. Rev. Plant Physiol. Plant Mol. Biol.* **48**, 641–672 (1997).
21. K. Satoh In *The Photosynthetic Reaction Center*, Vol. 1, J. Deisenhofer and J. R. Norris (Eds.), pp 289–318, Academic, San Diego (1993).
22. M. Seibert In *The Photosynthetic Reaction Center*, Vol. 1, J. Deisenhofer and J. R. Norris (Eds.), pp. 319–356, Academic, San Diego (1993).
23. K. D. Irrgang, L. X. Shi, C. Funk, W. P. Schröder. *J. Biol. Chem.* **270**, 17588–17593 (1995).
24. C. Eijckelhoff and J. P. Dekker. *Biochim. Biophys. Acta* **1231**, 21–28 (1995).
25. W. R. Newell, H. van Amerongen, J. Barber, R. van Grondelle. *Biochim. Biophys. Acta* **1057**, 232–238 (1991).
26. R. N. Frese, M. Germano, F. L. de Weerd, I. H. M. van Stokkum, A. Y. Shkuropatov, V. A. Shuvalov, H. J. van Gorkom, R. van Grondelle, J. P. Dekker. *Biochemistry* **42**, 9205–9213 (2003).
27. I. Renge, R. van Grondelle, J. Dekker. *J. Photochem. Photobiol.* **6**, 109 (1996).
28. N. Holt, J. T. M. Kennis, G. R. Fleming. *J. Phys. Chem. B* **108**, 19029–19035 (2004).

29. J. Koepke, X. Hu, C. Muenke, K. Schulten, H. Michel. *Structure* **4**, 581–597 (1996).
30. G. McDermott, S. M. Prince, A. A. Freer, A. M. Hawthornthwaite-Lawless, M. Z. Papiz, R. J. Cogdell. *Nature* **374**, 517 (1995).
31. A. N. Macpherson, J. B. Arellano, N. J. Fraser, R. J. Cogdell, T. Gillbro. *Biophys. J.* **80**, 923–930 (2001).
32. B. P. Krueger, G. D. Scholes, R. Jimenez, G. R. Fleming. *J. Phys. Chem. B* **102**, 2284–2292 (1998).
33. B. P. Krueger, J. Yom, P. J. Walla, G. R. Fleming. *Chem. Phys. Lett.* **310**, 57–64 (1999).
34. P. J. Walla, J. Yom, B. P. Krueger, G. R. Fleming. *J. Phys. Chem. B* **104**, 4799–4806 (2000).
35. B. P. Krueger, G. D. Scholes, G. R. Fleming. *J. Phys. Chem. B* **102**, 5378–5386 (1998).
36. M. Petersilka, U. J. Gossmann, E. K. U. Gross. *Phys. Rev. Lett.* **76**, 1212–1215 (1996).
37. C.-P. Hsu, P. J. Walla, M. Head-Gordon, G. R. Fleming. *J. Phys. Chem. B* **105**, 11016–11025 (2001).
38. D. L. Dexter. *J. Chem. Phys.* **21**, 836–850 (1953).
39. E. Hofmann, P. M. Wrench, F. P. Sharples, R. G. Hiller, W. Welte, K. Diederichs. *Science* **272**, 1788–1791 (1996).
40. J. A. Bautista, R. E. Connors, B. B. Raju, R. G. Hiller, F. P. Sharples, D. Gosztola, M. R. Wasielewski, H. A. Frank. *J. Phys. Chem. B* **103**, 8751–8758 (1999).
41. H. A. Frank, J. A. Bautista, J. Josue, Z. Pendon, R. G. Hiller, F. P. Sharples, D. Gosztola, M. R. Wasielewski. *J. Phys. Chem. B* **104**, 4569–4577 (2000).
42. D. Zigmantas, T. Polivka, R. G. Hiller, A. Yartsev, V. Sundstrom. *J. Phys. Chem. A* **105**, 10296–10306 (2001).
43. D. Zigmantas, R. G. Hiller, V. Sundstrom, T. Polivka. *Proc. Natl. Acad. Sci. USA* **99**, 16760–16765 (2002).
44. S. Akimoto, S. Takaishi, T. Ogata, Y. Nishimura, I. Yamazaki, M. Mimuro. *Chem. Phys. Lett.* **260**, 147–152 (1996).
45. H. M. Vaswani, C.-P. Hsu, M. Head-Gordon, G. R. Fleming. *J. Phys. Chem. B* **107**, 6500–6503 (2003).
46. J. Zimmermann, P. A. Linden, H. M. Vaswani, R. G. Hiller, G. R. Fleming. *J. Phys. Chem. B* **106**, 9418–9423 (2002).
47. P. A. Linden, J. Zimmermann, T. Brixner, N. E. Holt, H. M. Vaswani, R. G. Hiller, G. R. Fleming. *J. Phys. Chem. B* **108**, 10340–10345 (2004).
48. S. Shima, R. P. Ilagan, N. Gillespie, B. J. Sommer, R. G. Hiller, F. P. Sharples, H. A. Frank, R. R. Birge. *J. Phys. Chem. A* **107**, 8052 (2003).
49. C.-P. Hsu, X. Song, R. A. Marcus. *J. Phys. Chem. B* **101**, 2546–2551 (1997).
50. T. Polívka, J. L. Herek, D. Zigmantas, H.-E. Åkerlund, V. Sundström. *Proc. Natl. Acad. Sci. USA* **96**, 4914–4917 (1999).
51. T. Polivka, D. Zigmantas, H. A. Frank, J. A. Bautista, J. L. Herek, Y. Koyama, R. Fujii, V. Sundstroem. *J. Phys. Chem. B* **105**, 1072–1080 (2001).
52. T. Polívka, D. Zigmantas, J. L. Herek, Z. He, T. Pascher, T. Pulleruts, R. J. Cogdell, H. A. Frank, V. Sundström. *J. Phys. Chem. B* **106**, 11016–11025 (2002).
53. E. Papagiannakis, I. H. M. van Stokkum, R. van Grondelle, R. A. Niederman, D. Zigmantas, V. Sundstroem, T. Polivka. *J. Phys. Chem. B* **107**, 11216–11223 (2003).
54. D. Zigmantas, R. G. Hiller, F. P. Sharples, H. A. Frank, V. Sundstroem, T. Polivka. *Phys. Chem. Chem. Phys.* **6**, 3009–3016 (2004).
55. J. Barber and B. Andersson. *Trends Biochem. Sci.* **17**, 61–66 (1992).
56. K. K. Niyogi. *Annu. Rev. Plant Physiol. Plant Mol. Biol.* **50**, 333–359 (1999).
57. P. Müller, X.-P. Li, K. K. Niyogi. *Plant Physiol.* **125**, 1558–1566 (2001).
58. X.-P. Li, P. Müller-Moulé, A. M. Gilmore, K. K. Niyogi. *Proc. Natl. Acad. Sci. USA* **99**, 15222–15227 (2002).

59. N. Holt, G. R. Fleming, K. K. Niyogi. *Biochemistry* **43**, 8281–8289 (2004).
60. M. Havaux and K. K. Niyogi. *Proc. Natl. Acad. Sci. USA* **96**, 8762–8767 (1999).
61. B. Demmig-Adams, W. W. Adams III, D. H. Barker, B. A. Logan, D. R. Bowling, A. S. Verhoeven. *Physiol. Plant.* **98**, 253–264 (1996).
62. R. Bassi and S. Caffarri. *Photosynth. Res.* **64**, 243–256 (2000).
63. X.-P. Li, O. Björkman, C. Shih, A. R. Grossman, M. Rosenquist, S. Jansson, K. K. Niyogi. *Nature* **403**, 391–395 (2000).
64. B. Demmig-Adams and W. W. Adams III. *Trends Plant Sci.* **1**, 21–26 (1996).
65. P. Horton, A. V. Ruban, R. G. Walters. *Annu. Rev. Plant Phys.* **47**, 655–684 (1996).
66. B. Demmig-Adams. *Biochim. Biophys. Acta* **1020**, 1–24 (1990).
67. T. G. Owens, A. P. Shreve, A. C. Albrecht. *Dynamics and Mechanism of Singlet Energy Transfer Between Carotenoids and Chlorophylls: Light Harvesting and Nonphotochemical Fluorescence Quenching*, Vol. 4, Kluwer Academic, Dordrecht (1992).
68. H. A. Frank, A. Cua, V. Chynwat, A. Young, D. Gosztola, M. R. Wasielewski. *Photosynth. Res.* **41**, 389–395 (1994).
69. H. A. Frank, J. A. Bautista, J. S. Josue, A. J. Young. *Biochemistry* **39**, 2831–2837 (2000).
70. J. S. Josue and H. A. Frank. *J. Phys. Chem. A* **106**, 4815–4824 (2002).
71. P. Horton, A. V. Ruban, M. Wentworth. *Philos. Trans. R. Soc. London B* **355**, 1361–1370 (2000).
72. Y.-Z. Ma, N. E. Holt, X.-P. Li, K. K. Niyogi, G. R. Fleming. *Proc. Natl. Acad. Sci. USA* **100**, 4377–4382 (2003).
73. A. Dreuw, G. R. Fleming, M. Head-Gordon. *J. Phys. Chem. B* **107**, 6500–6503 (2003).
74. A. Dreuw, G. R. Fleming, M. Head-Gordon. *Phys. Chem. Chem. Phys.* **5**, 3247–3256 (2003).
75. P. Jordan, P. Fromme, H. T. Witt, O. Klukas, W. Saenger, N. Krauss. *Nature* **411**, 909–917 (2001).
76. H. M. Vaswani, M. Yang, A. Damjanovic, G. R. Fleming. *Proceedings of Femtochemistry VI, Ultrafast Molecular Events in Chemistry and Biology* (2004).
77. M. Yang, A. Damjanovic, H. M. Vaswani, G. R. Fleming. *Biophys. J.* **85**, 140–158 (2003).
78. M. Yang and G. R. Fleming. *J. Chem. Phys.* **119**, 5614–5622 (2003).
79. A. Damjanovic, H. M. Vaswani, P. Fromme, G. R. Fleming. *J. Phys. Chem. B* **106**, 10251–10261 (2002).
80. W. M. Zhang, T. Meier, V. Chernyak, S. Mukamel. *J. Chem. Phys.* **108**, 7763–7774 (1998).
81. M. Yang and G. R. Fleming. *Chem. Phys.* **282**, 163–180 (2002).
82. T. Joo, Y. Jia, J.-Y. Yu, M. J. Lang, G. R. Fleming. *J. Chem. Phys.* **104**, 6089–6108 (1996).
83. M. Cho, J.-Y. Yu, T. Joo, Y. Nagasawa, S. A. Passino, G. R. Fleming. *J. Phys. Chem.* **100**, 11944–11953 (1996).
84. M. Yang and G. R. Fleming. *J. Chem. Phys.* **110**, 2983–2990 (1999).
85. R. Agarwal, B. S. Prall, A. H. Rizvi, M. Yang, G. R. Fleming. *J. Chem. Phys.* **116**, 6243–6252 (2002).
86. R. Agarwal, B. S. Prall, A. H. Rizvi, M. Yang, G. R. Fleming. In *Ultrafast Phenomena XIII*, R. J. D. Miller, M. M. Murnane, N. F. Scherer, A. M. Weiner (Eds.), pp. 532–534, Springer, Berlin (2003).
87. B. S. Prall, D. Y. Parkinson, M. Yang, N. Ishikawa, G. R. Fleming. *J. Chem. Phys.* **120**, 2537 (2004).
88. M. Yang, R. Agarwal, G. R. Fleming. *J. Photochem. Photobiol. A: Chem.* **142**, 107–119 (2001).
89. H. van Amerongen, L. Valkunas, R. van Grondelle. *Photosynthetic Excitons*, World Scientific, Singapore (2000).
90. G. R. Fleming and G. D. Scholes. *Nature* **431**, 256–257 (2004).
91. G. D. Scholes and G. R. Fleming. In *Adv. Chem. Phys.* In press.
92. T. Brixner, T. Mancal, I. Stiopkin, G. R. Fleming. *J. Chem Phys.* **121**, 4221–4236 (2004).
93. M. L. Cowan, J. P. Ogilvie, R. J. D. Miller. *Chem. Phys. Lett.* **386**, 184 (2004).
94. A. Aspuru-Guzik, O. El-Akramine, W. A. Lester. *J. Chem. Phys.* **120**, 3049–3050 (2003).

95. B. L. Hammond, W. A. Lester, P. J. Reynolds. *Monte Carlo Methods in Ab Initio Quantum Chemistry,* World Scientific, Singapore (1994).
96. O. El Akramine, A. C. Kollias, W. A. Lester. *J. Chem Phys.* **119**, 1483 (2003).
97. P. J. Reynolds, D. M. Ceperley, B. J. Alder, W. A. Lester. *J. Chem Phys.* **77**, 5593 (1982).